[^{89}Zr]Zr(oxinate)$_4$ allows direct radiolabelling and PET imaging of small extracellular vesicles

Azalea Khan[1], Francis Man[1,2], Farid Faruqu[2], Jana Kim[1], Fahad Al-Salemee[1], Alessia Volpe[1,3], Gilbert Fruhwirth[1], Khuloud Al-Jamal[2], and Rafael T. M. de Rosales[1]

[1] *Department of Imaging Chemistry and Biology, School of Biomedical Engineering and Imaging Sciences, King's College London, St. Thomas' Hospital, London*

[2] *Institute of Pharmaceutical Sciences, School of Cancer & Pharmaceutical Sciences, King's College London, Franklin Wilkins Building, London*

[3] *Molecular Imaging Group, Department of Radiology, Memorial Sloan Kettering Cancer Centre, New York*

Abstract

[^{89}Zr]Zr(oxinate)$_4$ allows direct radiolabelling of exosomes/small extracellular vesicles (sEVs) and *in vivo* PET-CT imaging.

Graphical Abstract

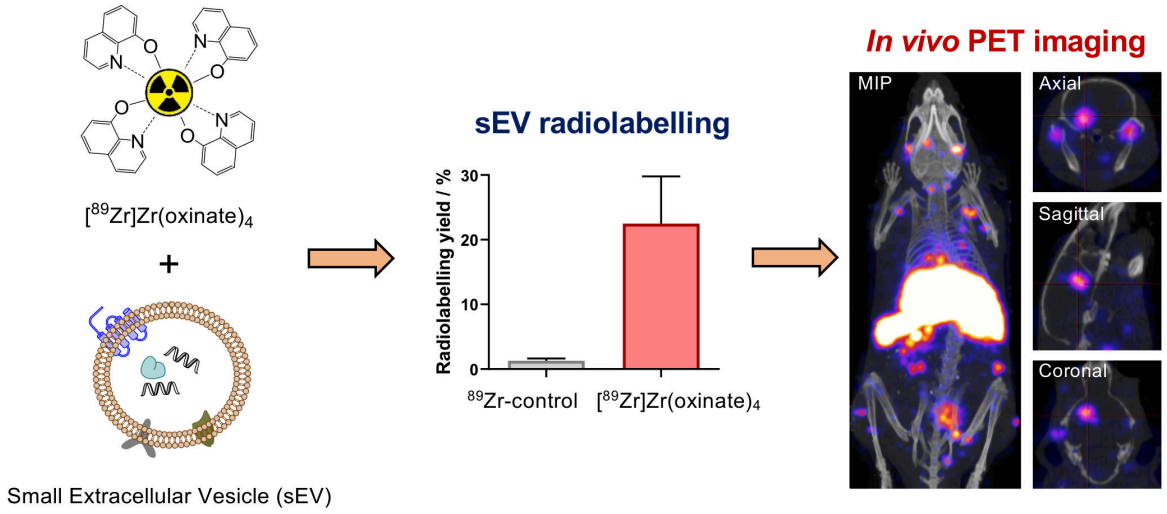

Introduction

Exosomes, better described as small extracellular vesicles (sEVs),[1] are cell-derived nanovesicles enclosed by a phospholipid bilayer, secreted by most cell types.[2] They are formed inside endosomal multivesicular bodies and are released into the extracellular space by exocytosis. One of the common features of sEVs are their small size, with hydrodynamic diameters in the 30–150 nm range. They are characterised by the presence of specific membrane marker proteins such as CD63, CD9, Alix and TSG101.[3] The role of sEVs is the transport and exchange of cytosolic molecules, such as nucleic acids, lipids and proteins between cells,[4] thus acting as messengers in cell-cell communication and disease progression.[5] For example, tumour cell-derived sEVs have been shown to promote tumour cell proliferation,[6] metastasis,[7] and induce anticancer drug resistance.[8] Interestingly, both natural and drug-loaded sEVs (derived from stem cells, immune cells or cancer cells) have shown therapeutic potential in diseases such as cancer,[9] Alzheimer's disease,[10] and type 2 diabetes.[11] Furthermore, they have the ability to cross the blood-brain barrier (BBB),[12] and to selectively target different tissues.[13] Therefore, there is an increasing interest in the use of sEVs as nanotherapeutics.[14] In this context, it is important to develop imaging tools that track the *in vivo* behaviour of sEVs. Doing so will not only improve our understanding of their biology, but also potentially maximise their application as nanotheranostic tools.

Optical imaging has been employed to investigate the distribution of cell-derived sEVs,[15-18] but with associated challenges in quantification and signal tissue penetration. Radionuclide imaging can easily overcome these limitations. In particular, positron emission tomography (PET) imaging allows highly sensitive and quantitative whole-body imaging, with no background signal and unlimited tissue penetration in both animals and humans.[19] At the time of writing, there are only a handful of peer-reviewed publications on the radiolabelling and *in vivo* imaging of sEVs,[18, 20-28] of which only 3 were aimed for PET imaging using two different radioisotopes (^{64}Cu and ^{124}I).[26-28] These PET radiolabelling methods rely on the binding of these radionuclides to membrane proteins which, given the importance of these surface components in the role of sEVs as messengers and cell-cell communication,[29] may result in altered biodistribution and function.[20, 28, 30] Consequently, we believe that radiolabelling within the intraluminal space of sEVs is preferable.

Based on our previous work on cell and liposomal nanomedicine radiolabelling,[31-33] we hypothesised that radiometal complexes that are metastable, lipophilic, and neutral, such as those based on ionophore ligands, would allow intraluminal sEV radiolabelling. In particular, we have recently shown that the PET radionuclide ^{89}Zr, complexed by 8-hydroxyquinoline (8-HQ or *oxine*) allows direct radiolabelling of liposomes demonstrating intraluminal delivery of ^{89}Zr across the lipid bilayer of vesicles.[34] Here, we report a radiochemical synthesis method of [^{89}Zr]Zr(oxinate)$_4$ that allows efficient radiolabelling of sEVs and *in vivo* tracking in mice using PET imaging.

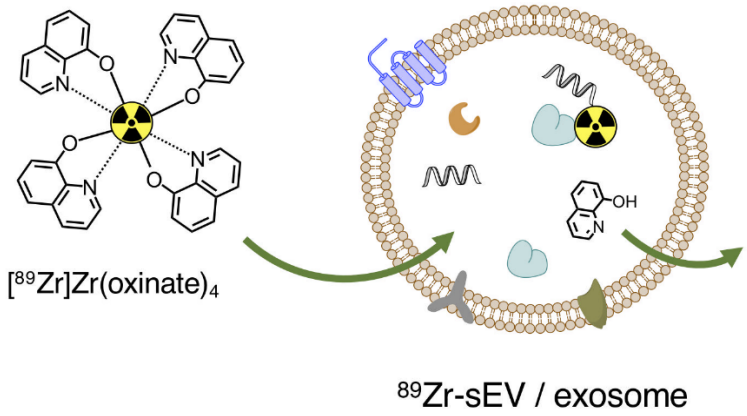

Scheme 1. Schematic representation of the intraluminal ^{89}Zr radiolabelling strategy of sEVs. The lipophilic [^{89}Zr]Zr(oxinate)$_4$ complex is able to pass through the lipid bilayer of the vesicles where ^{89}Zr dissociates from the oxine ligands (that presumably become protonated and are able to cross the lipid bilayer) and ^{89}Zr binds to intravesicular metal chelating ligands, such as proteins and nucleic acids within the sEV.

Results and Discussion

[^{89}Zr]Zr(oxinate)$_4$ synthesis was optimised to allow sEV radiolabelling (**Fig. 1A**). In particular, the final solution has to be isosmotic to avoid sEV damage and with a high ^{89}Zr concentration for *in vivo* PET imaging studies. To achieve this our synthesis involved the conversion of [^{89}Zr]Zr(oxalate)$_4$ in 1M oxalic acid, as received from cyclotron production, into [^{89}Zr]ZrCl$_4$ (in 1M HCl) by ion exchange chromatography.[35] This was followed by a drying step involving gentle heating under a flow of N_2 gas to remove HCl and H_2O, allowing concentration of the radioactivity. At this point, 80 µL of a pH 7 buffered (HEPES) solution containing 40 µg (0.3 µmol) of oxine and 1 mg/mL polysorbate-80 as a surfactant were added (Method 1). To confirm the formation of [^{89}Zr]Zr(oxinate)$_4$, the solution was analysed using radiochromatography

(Whatman® Nº 1 cellulose and ethyl acetate). Using this system, [^{89}Zr]Zr(oxinate)$_4$ migrates to the solvent front (R_f = 1), whereas unreacted [^{89}Zr]ZrCl$_4$ stays at the origin (R_f = 0) (**Fig. 1B**). Performing the reaction at 4°C significantly improved the radiochemical yield (RCY) compared to room temperature (95.1 ± 2.6% *vs.* 85.7 ± 4.5%; p <0.0446; n = 3). Partition coefficient measurements (log$D_{7.4}$) are consistent with the formation of a neutral lipophilic [^{89}Zr]Zr(oxinate)$_4$ complex (**Fig. 1C**). [^{89}Zr]Zr(oxinate)$_4$ was also synthesised using an alternative method (Method 2) involving reaction of [^{89}Zr]ZrCl$_4$ with oxine as a solution in EtOH, followed by pH neutralisation (see supplementary methods). No significant difference in the radiochemical properties were observed between the two methods, based on RCY and log$D_{7.4}$ assessments (**Fig. S1**). However, radiolabelling of sEVs using Method 1 was found to be highly reproducible and stable. Hence, Method 1 was chosen for *in vivo* experiments.

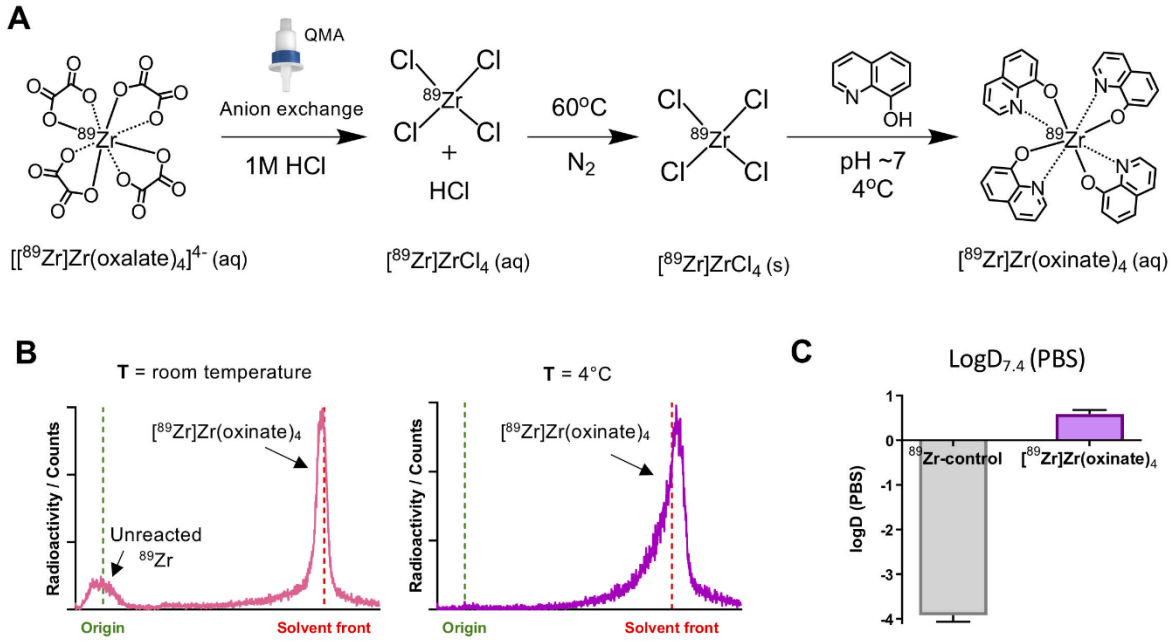

Figure 1: (A) Schematic representation of the [^{89}Zr]Zr(oxinate)$_4$ synthesis. **(B)** Radiochromatogram showing presence of unreacted ^{89}Zr when the reaction was performed at room temperature for 10 min, but not when at 4°C. **(C)** Log$D_{7.4}$(PBS) of control ^{89}Zr and [^{89}Zr]Zr(oxinate)$_4$ (n = 3).

As the release of sEVs from tumour cells is considerably higher than from normal cells,[36-38] we isolated sEVs from the cell culture supernatant of three cancer cell lines (B16.F10-GFP melanoma, MDA-MB-231.CD63-GFP breast cancer, and PANC1 pancreatic cancer cells) by precipitation or ultracentrifugation. Upon isolation, sEVs were characterised by size (using nanoparticle tracking analysis (NTA)) and their protein content was quantified (BCA assay). Additionally, MDA-MB-231.CD63-GFP and PANC1 sEVs were analysed by dot blot for expression of sEV markers CD63 and CD9. NTA revealed the average modal diameter for all three sEVs to be <150 nm, in compliance with the size range for sEVs (**Fig. S2**). The amount of protein detected in B16-F10.GFP sEVs was significantly higher than in both MDA-MB-231.CD63-GFP and PANC1 sEVs (**Fig. S3**), which could be due to by precipitation isolation employed to isolate the former sEV types.[39] Presence of CD63 and CD9 biomarkers was confirmed for both MDA-MB-231.CD63-GFP and PANC1 sEVs.

We then tested the sEV radiolabelling capabilities of [^{89}Zr]Zr(oxinate)$_4$. sEVs were incubated with [^{89}Zr]Zr(oxinate)$_4$ for 20 min at 37°C (**Fig. 2A**). These conditions were chosen based on our previous studies showing that [^{89}Zr]Zr(oxinate)$_4$ cell radiolabelling is temperature-independent and rapid (<20 min).[32] Following incubation, a small amount of the Zr chelator desferrioxamine (DFO) was added to scavenge any potential free $^{89}Zr^{4+}$ ions from the reaction solution, including those that may be weakly bound to the phospholipid membrane, as previously observed with liposomal vesicles.[40] The same sEV radiolabelling procedure was performed using non-chelated ^{89}Zr as a control (^{89}Zr-control). The reaction mixture was then passed through a size-exclusion chromatography (SEC) column (Sepharose® CL-2B)[20] that effectively separated sEVs from smaller molecules, including DFO-bound ^{89}Zr. The results, shown in **Fig. 2B**, demonstrate significantly higher radiolabelling yields with [^{89}Zr]Zr(oxinate)$_4$ compared to ^{89}Zr-control for all different sEVs, supporting our hypothesised radiolabelling strategy. Thus, [^{89}Zr]Zr(oxinate)$_4$ and not unchelated ^{89}Zr is able to pass through the lipid bilayer membrane into the intraluminal space of sEVs, where ^{89}Zr exchanges ligands and bind to intravesicular metal-chelating ligands, as we have previously demonstrated in cells and liposomes.[32-34] Importantly, there was no significant change in the hydrodynamic size of B16-F10.GFP and PANC1 sEVs before and after radiolabelling, unlike MDA-MB-231.CD63-GFP sEVs (**Fig. 2C**). However, there was no significant change in the expression of sEV markers CD63 and CD9 before and after radiolabelling of MDA-MB-231.CD63-GFP and PANC1 sEVs (**Fig. 2D**). Taking all these results into account, and the higher RLY achieved (**Fig. S4**), PANC1 sEVs were chosen for further *in vitro* and *in vivo* experiments.

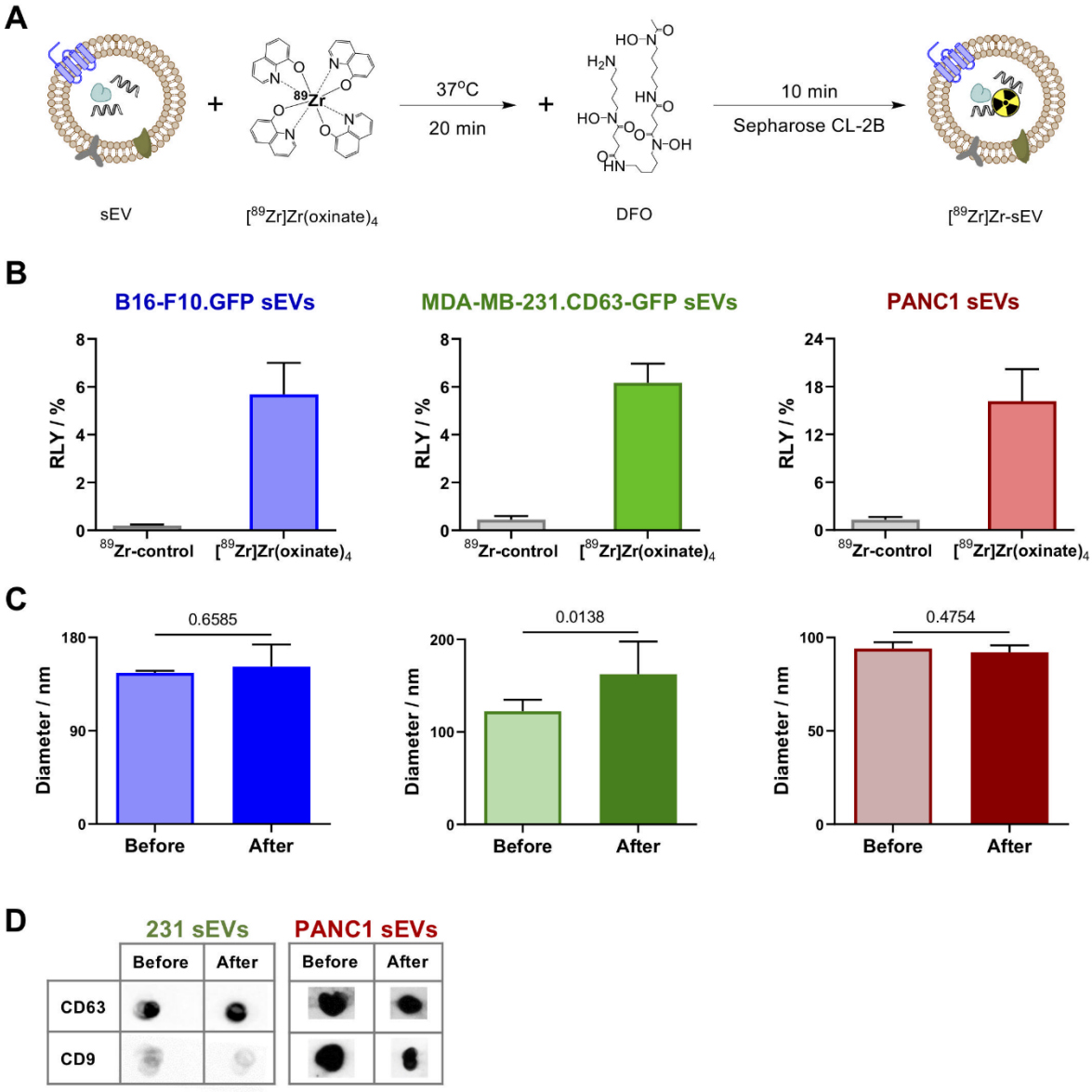

Figure 2. (A) Schematic representation of the sEV radiolabelling protocol using [^{89}Zr]Zr(oxinate)$_4$. **(B)** Radiolabelling yield (RLY) of 1x10^{10} B16-F10.GFP sEVs (blue) = 5.7 ± 1.3%, 1x10^{10} MDA-MB-231.CD63-GFP sEVs (green) = 6.2 ± 0.8%, and 1x10^{11} PANC1 sEVs (maroon) = 16.2 ± 4.0%; (n = 3). **(C)** NTA data showing the hydrodynamic diameter of respective sEVs before and after radiolabelling, analysed by Student's unpaired t-test. **(D)** CD63 and CD9 expression of 231 and PANC1 sEVs by dot blot before and after radiolabelling.

Radiochemical stability of ^{89}Zr-PANC1 sEVs was assessed in human serum at 37°C using SEC (Sepharose). However, we found that this system resulted in losses of *ca.* 80% of vesicles in the column (data not shown). Hence, we took an alternative approach to evaluate the *in vitro* stability that included testing the ability of ^{89}Zr-PANC1 sEVs to be taken up by cells. Thus, ^{89}Zr-PANC1 sEVs, [^{89}Zr]Zr(oxinate)$_4$ or ^{89}Zr-control were incubated at 37°C in serum supplemented cell media with the following cells: PANC1 (parental cells), HEK-293T (healthy cells with known nanoparticle uptake properties),[41] MDA-MB-231 and DU-145 (non-parental cancer cells). Interestingly, ^{89}Zr uptake by both PANC1 cells and HEK-293T cells was significantly higher for the ^{89}Zr-PANC1 sEV group, compared to the two control groups (**Fig. 3A-B**). In contrast, there were very low levels of ^{89}Zr-PANC1-sEV uptake by the non-parental cancer cell lines (**Fig. 3C-D**). It is worth highlighting the higher uptake of ^{89}Zr-PANC1-sEVs in both PANC1 and HEK-293T cells compared to that achieved by [^{89}Zr]Zr(oxinate)$_4$, taking into account that the latter has proven cell-radiolabelling properties.[32, 42] Thus, these data suggest that ^{89}Zr-PANC1-sEVs are stable at 37°C in serum containing media, and demonstrate quick uptake by both parental cells and HEK-293T cells, but not by other non-parental cancer cells.

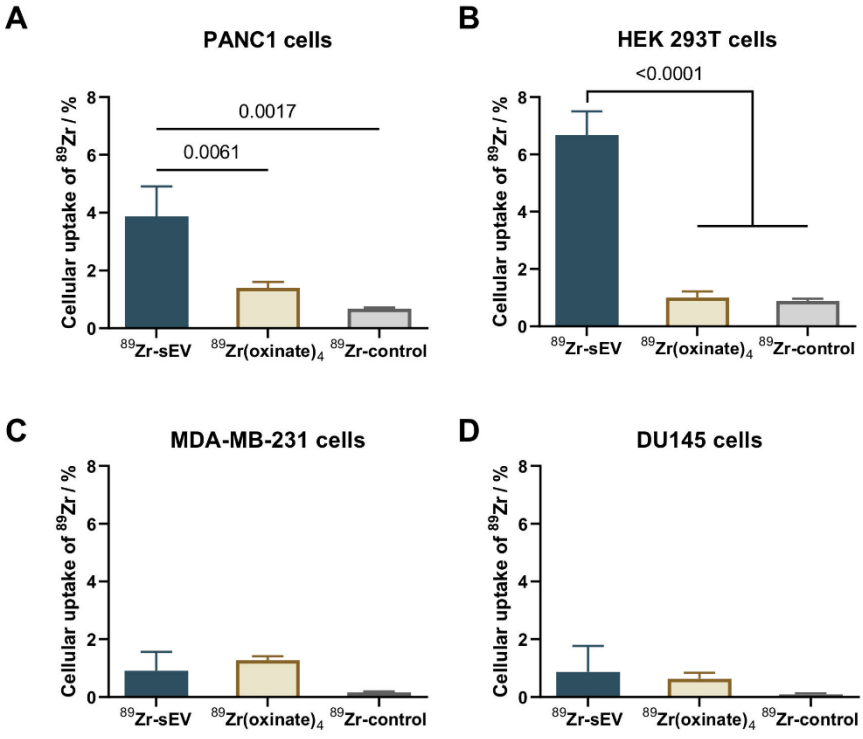

Figure 3: *In vitro* uptake of ^{89}Zr-PANC1 sEVs by (**A)** parental PANC1 cells, (**B)** HEK 293T cells, (**C)** MDA-MB-231 cells, and **D)** DU145 cells after co-incubation in serum supplemented media for 4 h. The final cell uptake data were normalised for 50,000 cells. Data given as mean ± SD of n = 3 and analysed by one-way ANOVA with Turkey's correction for multiple comparisons.

Encouraged by these results, we performed an *in vivo* PET-CT imaging and biodistribution study of PANC1 sEVs in healthy mice (C57BL/6). To assess the impact of damaged vesicles on the imaging of sEVs, we evaluated two groups: (*i*) intact ^{89}Zr-PANC1 sEVs and (*ii*) heat-damaged ^{89}Zr-PANC1 sEVs. The heat damage protocol consisted of two cycles of heating-cooling (90°C to 0°C) ^{89}Zr-PANC1 sEVs, and aimed at denaturing the vesicles, but avoiding complete breakdown. Indeed, the heat damage process resulted in a significant increase in size and partial release of internal contents compared to intact ^{89}Zr-PANC1 sEVs (**Fig. S5**). ^{89}Zr-PANC1 sEVs were prepared with a RLY of 32% (starting with 1 x 10^{12} sEVs). PET-CT imaging within 1 h post intravenous (iv.) injection (~1 x 10^{10} sEVs/mouse), showed short circulation times and rapid uptake of intact ^{89}Zr-PANC1 sEVs in the liver, spleen, bladder, as well as several lymph nodes (LN) and brain (**Fig. 4A i**). Short circulation times, liver/spleen as well as bladder uptake have been observed in other imaging studies of sEV biodistribution *via* iv. administration.[16-18, 20, 21, 25-27, 43] However, to the best of our knowledge, this is the first time LN uptake is observed using *in vivo* imaging. With the help of CT imaging, the PET signals observed from the suspected LNs can be correlated with their well-documented location in mice (*e.g.* cervical, brachial, pancreatic, renal, inguinal, popliteal, and others; **Fig. S6**). sEV/exosome uptake in secondary lymphoid organs (*i.e.* spleen and LNs) following iv. injection in the same mouse strain has been recently demonstrated, and is mediated by CD169^{+} macrophages.[44] Interestingly, sEVs are known to express α-2,3-linked sialic acid, which is the preferred ligand of CD169 thus providing a plausible explanation for the high spleen and LN uptake observed.[45] The possibility of these imaging signals being due to released free ^{89}Zr seems improbable due to its significantly different biodistribution (same mouse strain and timing; data courtesy of Ma *et al.*[46]) (**Fig. 4A iii**). In addition, ^{89}Zr-PANC1 sEVs were visible within the brain (**Fig. 4B**), supporting the previously reported ability of sEVs to cross the BBB.[12, 47] Heat-damaged ^{89}Zr-PANC1 sEVs showed a similar biodistribution to intact ^{89}Zr-PANC1 sEVs, with the major differences being a significantly lower spleen uptake and a higher bone signal (**Fig. 4A ii**). These two findings can be explained by the bigger size of the denatured vesicles and partial release of contents, as a result of the heat damaging process. In both groups bone signal increased at 24 h post injection, as expected due to the metabolic activity in the liver/spleen that will result in the release of bone-tropic 'free' ^{89}Zr. In addition, fewer lymph nodes were visible and no brain signal was observed.

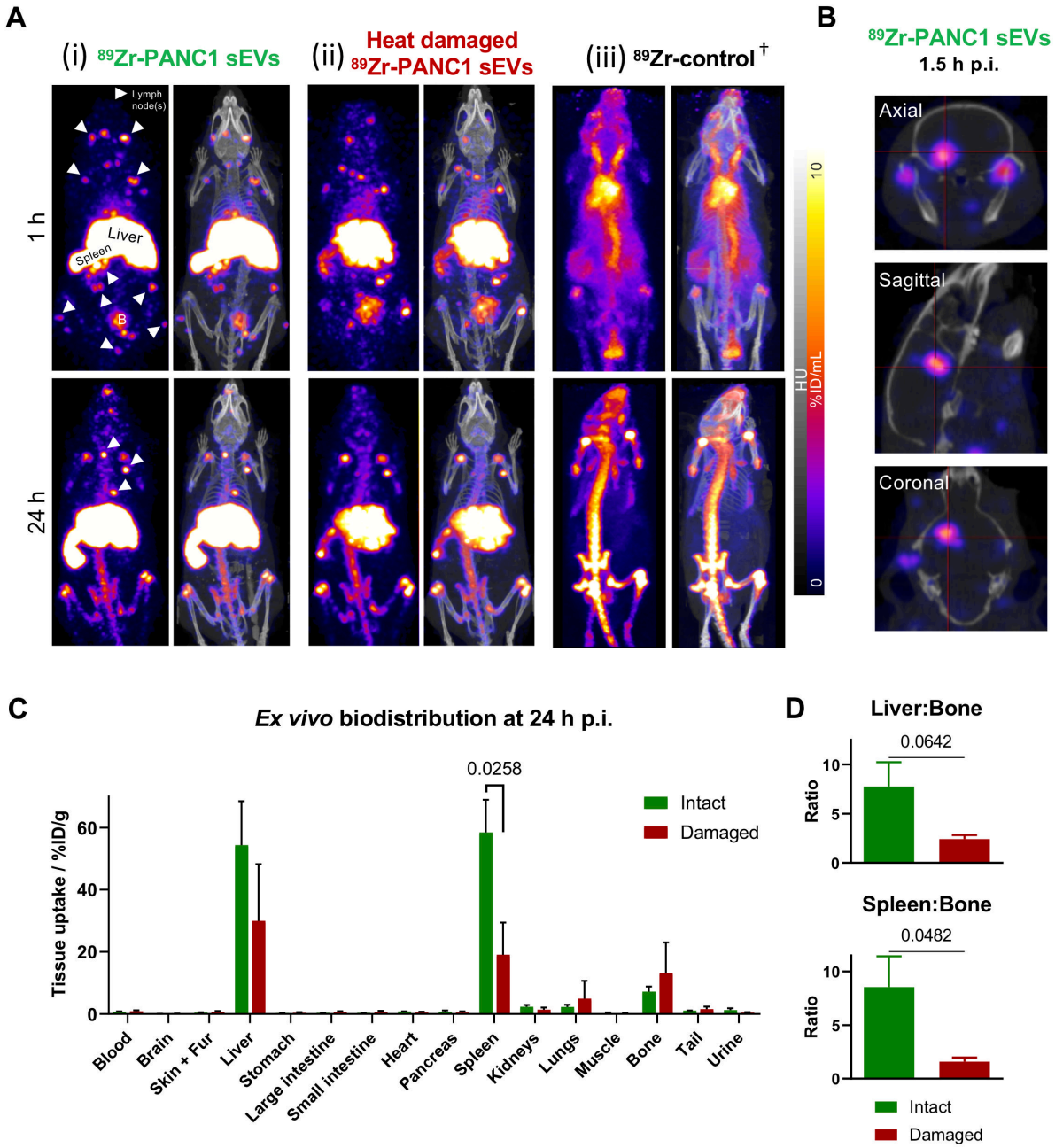

Figure 4. (A) Maximum intensity projection PET-CT images of **(i)** intact ^{89}Zr-PANC1 sEVs, **(ii)** heat-damaged ^{89}Zr-PANC1 sEVs, and **(iii)** neutralised $^{89}Zr^{4+}$ biodistribution in a C57BL/6 mouse at 1 h and 24 h post-intravenous injection; white arrowheads = representative lymph nodes (see Fig S6), B = bladder, † = PET image scale for control ^{89}Zr at 1 h is 10 times that of the other images; the scale had to be adjusted for image clarity. **B)** PET-CT images (axial, sagittal and coronal slices) of a mouse injected with intact ^{89}Zr-PANC1 sEVs showing uptake within the brain; image scale is the same as in (A). **(C)** *Ex vivo* biodistribution showing uptake of "intact" (n = 3) and "heat-damaged" (n = 2) ^{89}Zr-PANC1 sEVs. **D)** Ratio of liver:bone uptake (n = 3) and spleen:bone uptake (n = 2); data given as the geometrical mean ± SD of the n values. Statistical significances were calculated using Student's unpaired t-test.

The PET-CT imaging findings correlated well with the *ex vivo* biodistribution data at 24 h post injection, showing high liver/spleen signal and significantly higher uptake of intact ^{89}Zr-PANC1 sEVs in the spleen (58.5 ± 10.5 %ID/g) compared to heat-damaged ^{89}Zr-PANC1 sEVs (19.1 ± 10.3 %ID/g), p = 0.0258 **(Fig. 4C)**. Liver uptake was also higher for intact ^{89}Zr-PANC1 sEVs, whereas bone uptake was higher for heat-damaged ^{89}Zr-PANC1 sEVs. These two latter findings are consistent with the imaging studies discussed above but the differences were not statistically significant. However, differential uptake of intact *vs.* heat-damaged ^{89}Zr-PANC1 sEVs was observed when looking at the liver:bone (7.7 ± 2.5 *vs.* 2.4 ± 0.4, respectively) and spleen:bone (8.6 ± 2.9 *vs.* 1.6 ± 0.4, respectively) uptake ratios, suggesting a potential role of these as imaging biomarkers for assessing the *in vivo* stability of radiolabelled sEVs **(Fig. 4D)**.

In summary, we have developed and optimised the synthesis of [^{89}Zr]Zr(oxinate)$_4$ for sEV radiolabelling and demonstrated that this radiotracer allows for a simple, efficient and direct radiolabelling method for sEVs. Unlike previously reported sEV PET radiolabelling methods, [^{89}Zr]Zr(oxinate)$_4$ targets the internal components, avoiding potential modification of surface biomolecules. PET-CT imaging of ^{89}Zr-PANC1 sEVs showed ^{89}Zr uptake in liver, spleen, brain, as well as suspected accumulation in lymph nodes, according to their location. We have also demonstrated that heat-damaged ^{89}Zr-PANC1 sEVs show significant differences in spleen uptake, and liver:bone and spleen:bone uptake ratios that have potential as imaging biomarkers for sEV stability. Using PANC1 cell derived sEVs as a model, our results demonstrate that [^{89}Zr]Zr(oxinate)$_4$ is an efficient radiolabelling agent for sEVs. Further work will be aimed at understanding the nature of the extensive lymph node and brain ^{89}Zr uptake, and using PET imaging to study the potential role of sEVs as nanotheranostics. We believe this radiochemical tool will help the sEV field to further investigate their *in vivo* behaviour, to answer questions on their basic biology as well as explore their potential as disease biomarkers and therapeutics.

Acknowledgements:

The authors would like to thank Dr Oskar Timmermand for assistance during dissection, and Dr Tim Witney for a loan of a 4-mouse hotel for preclinical PET/CT imaging. Azalea Khan is

supported by the UK Medical Research Council (MRC) [MR/N013700/1] and King's College London MRC Doctoral Training Partnership in Biomedical Sciences. This work was also funded by EPSRC programme grants EP/S032789/1 and EP/R045046/1 and the Wellcome/EPSRC Centre for Medical Engineering [WT/203148/Z/16/Z]. We also acknowledge support from the KCL and UCL Comprehensive Cancer Imaging Centre funded by CRUK and EPSRC in association with the MRC and DoH (England). PET scanning equipment at KCL was funded by an equipment grant from the Wellcome Trust under grant number WT 084052/Z/07/Z. Radioanalytical equipment was funded by a Wellcome Trust Multi User Equipment Grant: A multiuser radioanalytical facility for molecular imaging and radionuclide therapy research. The authors finally acknowledge support the National Institute for Health Research (NIHR) Biomedical Research Centre based at Guy's and St Thomas' NHS Foundation Trust and KCL [grant number IS-BRC-1215-20006]. The views expressed are those of the authors and not necessarily those of the NHS, the NIHR or the Department of Health.

References

1. C. Théry, K. W. Witwer, E. Aikawa, M. J. Alcaraz, J. D. Anderson, R. Andriantsitohaina, A. Antoniou, T. Arab, F. Archer, G. K. Atkin-Smith, D. C. Ayre, J.-M. Bach, D. Bachurski, H. Baharvand, L. Balaj, S. Baldacchino, N. N. Bauer, A. A. Baxter, M. Bebawy, C. Beckham, A. Bedina Zavec, A. Benmoussa, A. C. Berardi, P. Bergese, E. Bielska, C. Blenkiron, S. Bobis-Wozowicz, E. Boilard, W. Boireau, A. Bongiovanni, F. E. Borràs, S. Bosch, C. M. Boulanger, X. Breakefield, A. M. Breglio, M. Á. Brennan, D. R. Brigstock, A. Brisson, M. L. D. Broekman, J. F. Bromberg, P. Bryl-Górecka, S. Buch, A. H. Buck, D. Burger, S. Busatto, D. Buschmann, B. Bussolati, E. I. Buzás, J. B. Byrd, G. Camussi, D. R. F. Carter, S. Caruso, L. W. Chamley, Y.-T. Chang, C. Chen, S. Chen, L. Cheng, A. R. Chin, A. Clayton, S. P. Clerici, A. Cocks, E. Cocucci, R. J. Coffey, A. Cordeiro-da-Silva, Y. Couch, F. A. W. Coumans, B. Coyle, R. Crescitelli, M. F. Criado, C. D'Souza-Schorey, S. Das, A. Datta Chaudhuri, P. de Candia, E. F. De Santana, O. De Wever, H. A. del Portillo, T. Demaret, S. Deville, A. Devitt, B. Dhondt, D. Di Vizio, L. C. Dieterich, V. Dolo, A. P. Dominguez Rubio, M. Dominici, M. R. Dourado, T. A. P. Driedonks, F. V. Duarte, H. M. Duncan, R. M. Eichenberger, K. Ekström, S. El Andaloussi, C. Elie-Caille, U. Erdbrügger, J. M. Falcón-Pérez, F. Fatima, J. E. Fish, M. Flores-Bellver, A. Försönits, A. Frelet-Barrand, F. Fricke, G. Fuhrmann, S. Gabrielsson, A. Gámez-Valero, C. Gardiner, K. Gärtner, R. Gaudin, Y. S. Gho, B. Giebel, C. Gilbert, M. Gimona, I. Giusti, D. C. I. Goberdhan, A. Görgens, S. M. Gorski, D. W. Greening, J. C. Gross, A. Gualerzi, G. N. Gupta, D. Gustafson, A. Handberg, R. A. Haraszti, P. Harrison, H. Hegyesi, A. Hendrix, A. F. Hill, F. H. Hochberg, K. F. Hoffmann, B. Holder, H. Holthofer, B. Hosseinkhani, G. Hu, Y. Huang, V. Huber, S. Hunt, A. G.-E. Ibrahim, T. Ikezu, J. M. Inal, M. Isin, A. Ivanova, H. K. Jackson, S. Jacobsen, S. M. Jay, M. Jayachandran, G. Jenster, L. Jiang, S. M. Johnson, J. C. Jones, A. Jong, T. Jovanovic-Talisman, S. Jung, R. Kalluri, S.-i. Kano, S. Kaur, Y. Kawamura, E. T. Keller, D. Khamari, E. Khomyakova, A. Khvorova, P. Kierulf, K. P. Kim, T. Kislinger, M. Klingeborn, D. J. Klinke, M. Kornek, M. M. Kosanović, Á. F. Kovács, E.-M. Krämer-Albers, S. Krasemann, M. Krause, I. V. Kurochkin, G. D. Kusuma, S. Kuypers, S. Laitinen, S. M. Langevin, L. R. Languino, J. Lannigan, C. Lässer, L. C. Laurent, G. Lavieu, E. Lázaro-Ibáñez, S. Le Lay, M.-S. Lee, Y. X. F. Lee, D. S. Lemos, M. Lenassi, A. Leszczynska, I. T. S. Li, K. Liao, S. F. Libregts, E. Ligeti, R. Lim, S. K. Lim, A. Linē, K. Linnemannstöns, A. Llorente, C. A. Lombard, M. J. Lorenowicz, Á. M. Lörincz, J. Lötvall, J. Lovett, M. C. Lowry, X. Loyer, Q. Lu, B. Lukomska, T. R. Lunavat, S. L. N. Maas, H. Malhi, A. Marcilla, J. Mariani, J. Mariscal, E. S. Martens-Uzunova, L. Martin-Jaular, M. C. Martinez, V. R. Martins, M. Mathieu, S. Mathivanan, M. Maugeri, L. K. McGinnis, M. J. McVey, D. G. Meckes, K. L. Meehan, I. Mertens, V. R. Minciacchi, A. Möller, M. Møller Jørgensen, A. Morales-Kastresana, J. Morhayim, F. Mullier, M. Muraca, L. Musante, V. Mussack, D. C. Muth, K. H. Myburgh, T. Najrana, M. Nawaz, I. Nazarenko, P. Nejsum, C. Neri, T. Neri, R. Nieuwland, L. Nimrichter, J. P. Nolan, E. N. M. Nolte-'t Hoen, N. Noren Hooten, L. O'Driscoll, T. O'Grady, A. O'Loghlen, T. Ochiya, M. Olivier, A. Ortiz, L. A. Ortiz, X. Osteikoetxea, O. Østergaard, M. Ostrowski, J. Park, D. M. Pegtel, H. Peinado, F. Perut, M. W. Pfaffl, D. G. Phinney, B. C. H. Pieters, R. C. Pink, D. S. Pisetsky, E. Pogge von Strandmann, I. Polakovicova, I. K. H. Poon, B. H. Powell, I. Prada, L. Pulliam, P. Quesenberry, A. Radeghieri, R. L. Raffai, S. Raimondo, J. Rak, M. I. Ramirez, G. Raposo, M. S. Rayyan, N. Regev-Rudzki, F. L. Ricklefs, P. D. Robbins, D. D. Roberts, S. C. Rodrigues, E. Rohde, S. Rome, K. M. A. Rouschop, A. Rughetti, A. E. Russell, P. Saá, S. Sahoo, E. Salas-Huenuleo, C. Sánchez, J. A. Saugstad, M. J. Saul, R. M. Schiffelers, R. Schneider, T. H. Schøyen, A. Scott, E. Shahaj, S. Sharma, O. Shatnyeva, F. Shekari, G. V. Shelke, A. K. Shetty, K. Shiba, P. R. M. Siljander, A. M. Silva, A. Skowronek, O. L. Snyder, R. P. Soares, B. W. Sódar, C. Soekmadji, J. Sotillo, P. D. Stahl, W. Stoorvogel, S. L. Stott, E. F. Strasser, S. Swift, H. Tahara, M. Tewari, K. Timms, S. Tiwari, R. Tixeira, M. Tkach, W. S. Toh, R. Tomasini, A. C. Torrecilhas, J. P. Tosar, V. Toxavidis, L. Urbanelli, P. Vader, B. W. M. van Balkom, S. G. van der Grein, J. Van Deun, M. J. C. van Herwijnen, K. Van Keuren-Jensen, G. van Niel, M.

E. van Royen, A. J. van Wijnen, M. H. Vasconcelos, I. J. Vechetti, T. D. Veit, L. J. Vella, É. Velot, F. J. Verweij, B. Vestad, J. L. Viñas, T. Visnovitz, K. V. Vukman, J. Wahlgren, D. C. Watson, M. H. M. Wauben, A. Weaver, J. P. Webber, V. Weber, A. M. Wehman, D. J. Weiss, J. A. Welsh, S. Wendt, A. M. Wheelock, Z. Wiener, L. Witte, J. Wolfram, A. Xagorari, P. Xander, J. Xu, X. Yan, M. Yáñez-Mó, H. Yin, Y. Yuana, V. Zappulli, J. Zarubova, V. Žėkas, J.-y. Zhang, Z. Zhao, L. Zheng, A. R. Zheutlin, A. M. Zickler, P. Zimmermann, A. M. Zivkovic, D. Zocco and E. K. Zuba-Surma, *J. Extracell. Vesicles*, 2018, **7**, 1535750.

2. C. Thery, L. Zitvogel and S. Amigorena, *Nat. Rev. Immunol.*, 2002, **2**, 569-579.
3. M. Colombo, G. Raposo and C. Théry, *Annu. Rev. Cell Dev. Biol.*, 2014, **30**, 255-289.
4. G. Raposo and W. Stoorvogel, *J. Cell Biol.*, 2013, **200**, 373-383.
5. S. L. N. Maas, X. O. Breakefield and A. M. Weaver, *Trends Cell Biol.*, 2017, **27**, 172-188.
6. P. Zhang, H. Zhou, K. Lu, Y. Lu, Y. Wang and T. Feng, *OncoTargets Ther.*, 2018, **11**, 291-299.
7. A. Hoshino, B. Costa-Silva, T.-L. Shen, G. Rodrigues, A. Hashimoto, M. Tesic Mark, H. Molina, S. Kohsaka, A. Di Giannatale, S. Ceder, S. Singh, C. Williams, N. Soplop, K. Uryu, L. Pharmer, T. King, L. Bojmar, A. E. Davies, Y. Ararso, T. Zhang, H. Zhang, J. Hernandez, J. M. Weiss, V. D. Dumont-Cole, K. Kramer, L. H. Wexler, A. Narendran, G. K. Schwartz, J. H. Healey, P. Sandstrom, K. Jørgen Labori, E. H. Kure, P. M. Grandgenett, M. A. Hollingsworth, M. de Sousa, S. Kaur, M. Jain, K. Mallya, S. K. Batra, W. R. Jarnagin, M. S. Brady, O. Fodstad, V. Muller, K. Pantel, A. J. Minn, M. J. Bissell, B. A. Garcia, Y. Kang, V. K. Rajasekhar, C. M. Ghajar, I. Matei, H. Peinado, J. Bromberg and D. Lyden, *Nature*, 2015, **527**, 329.
8. F. M. Khan, E. Saleh, H. Alawadhi, R. Harati, W. H. Zimmermann and R. El-Awady, *Cancer Biol. Ther.*, 2018, **19**, 25-33.
9. S. Walker, S. Busatto, A. Pham, M. Tian, A. Suh, K. Carson, A. Quintero, M. Lafrence, H. Malik, M. X. Santana and J. Wolfram, *Theranostics*, 2019, **9**, 8001-8017.
10. T. Xiao, W. Zhang, B. Jiao, C. Z. Pan, X. Liu and L. Shen, *Transl. Neurodegener.*, 2017, **6**.
11. Y. Xiao, L. Zheng, X. Zou, J. Wang, J. Zhong and T. Zhong, *J. Extracell. Vesicles*, 2019, **8**, 1625677.
12. L. Alvarez-Erviti, Y. Seow, H. Yin, C. Betts, S. Lakhal and M. J. Wood, *Nat. Biotechnol.*, 2011, **29**, 341-345.
13. D. E. Murphy, O. G. de Jong, M. Brouwer, M. J. Wood, G. Lavieu, R. M. Schiffelers and P. Vader, *Exp. Mol. Med.*, 2019, **51**, 1-12.
14. O. M. Elsharkasy, J. Z. Nordin, D. W. Hagey, O. G. de Jong, R. M. Schiffelers, S. E. Andaloussi and P. Vader, *Adv Drug Deliv Rev*, 2020, DOI: 10.1016/j.addr.2020.04.004.
15. Y. Takahashi, M. Nishikawa, H. Shinotsuka, Y. Matsui, S. Ohara, T. Imai and Y. Takakura, *J. Biotechnol.*, 2013, **165**, 77-84.
16. C. P. Lai, O. Mardini, M. Ericsson, S. Prabhakar, C. Maguire, J. W. Chen, B. A. Tannous and X. O. Breakefield, *ACS Nano*, 2014, **8**, 483-494.
17. P. Zhang, B. Dong, E. Zeng, F. Wang, Y. Jiang, D. Li and D. Liu, *Anal. Chem.*, 2018, **90**, 11273-11279.
18. T. Smyth, M. Kullberg, N. Malik, P. Smith-Jones, M. W. Graner and T. J. Anchordoquy, *J. Control. Release*, 2015, **199**, 145-155.
19. M. L. James and S. S. Gambhir, *Physiol. Rev.,* 2012, **92**, 897-965.
20. F. N. Faruqu, J. T. Wang, L. Xu, L. McNickle, E. M. Chong, A. Walters, M. Gurney, A. Clayton, L. A. Smyth, R. Hider, J. Sosabowski and K. T. Al-Jamal, *Theranostics*, 2019, **9**, 1666-1682.
21. Z. Varga, I. Gyurko, K. Paloczi, E. I. Buzas, I. Horvath, N. Hegedus, D. Mathe and K. Szigeti, *Cancer Biother. Radiopharm.*, 2016, **31**, 168-173.
22. A. Matsumoto, Y. Takahashi, M. Nishikawa, K. Sano, M. Morishita, C. Charoenviriyakul, H. Saji and Y. Takakura, *Cancer Sci.*, 2017, **108**, 1803-1810.
23. M. Morishita, Y. Takahashi, M. Nishikawa, K. Sano, K. Kato, T. Yamashita, T. Imai, H. Saji and Y. Takakura, *J. Pharm. Sci.*, 2015, **104**, 705-713.
24. M. H. Rashid, T. F. Borin, R. Ara, K. Angara, J. Cai, B. R. Achyut, Y. Liu and A. S. Arbab, *Nanomedicine*, 2019, **21**, 102072.

25. M. I. González, P. Martín-Duque, M. Desco and B. Salinas, *Nanomaterials*, 2020, **10**, 1062.
26. S. Shi, T. Li, X. Wen, S. Y. Wu, C. Xiong, J. Zhao, V. R. Lincha, D. S. Chow, Y. Liu, A. K. Sood and C. Li, *Bioconjug. Chem.*, 2019, **30**, 2675-2683.
27. A. Banerjee, V. Alves, T. Rondão, J. Sereno, Â. Neves, M. Lino, A. Ribeiro, A. J. Abrunhosa and L. S. Ferreira, *Nanoscale*, 2019, **11**, 13243-13248.
28. F. Royo, U. Cossío, A. Ruiz de Angulo, J. Llop and J. M. Falcon-Perez, *Nanoscale*, 2019, **11**, 1531-1537.
29. Q. Hu, H. Su, J. Li, C. Lyon, W. Tang, M. Wan and T. Y. Hu, *Precis. Clin. Med.*, 2020, **3**, 54-66.
30. S. Rana, S. Yue, D. Stadel and M. Zoller, *Int. J. Biochem. Cell Biol.*, 2012, **44**, 1574-1584.
31. P. Gawne, F. Man, J. Fonslet, R. Radia, J. Bordoloi, M. Cleveland, P. Jimenez-Royo, A. Gabizon, P. J. Blower, N. Long and R. T. M. de Rosales, *Dalton Trans.*, 2018, **47**, 9283-9293.
32. F. Man, L. Lim, A. Volpe, A. Gabizon, H. Shmeeda, B. Draper, A. C. Parente-Pereira, J. Maher, P. J. Blower, G. O. Fruhwirth and R. T.M. de Rosales, *Mol. Ther.*, 2019, **27**, 219-229.
33. P. J. Gawne, F. Clarke, K. Turjeman, A. P. Cope, N. J. Long, Y. Barenholz, S. Y. A. Terry and R. T. M. de Rosales, *Theranostics*, 2020, **10**, 3867-3879.
34. S. Edmonds, A. Volpe, H. Shmeeda, A. C. Parente-Pereira, R. Radia, J. Baguna-Torres, I. Szanda, G. W. Severin, L. Livieratos, P. J. Blower, J. Maher, G. O. Fruhwirth, A. Gabizon and R. T. M. de Rosales, *ACS Nano*, 2016, **10**, 10294-10307.
35. J. P. Holland, Y. Sheh and J. S. Lewis, *Nucl. Med. Biol.*, 2009, **36**, 729-739.
36. D. D. Taylor and C. Gercel-Taylor, *Gynecol. Oncol.*, 2008, **110**, 13-21.
37. M. Logozzi, A. De Milito, L. Lugini, M. Borghi, L. Calabrò, M. Spada, M. Perdicchio, M. L. Marino, C. Federici, E. Iessi, D. Brambilla, G. Venturi, F. Lozupone, M. Santinami, V. Huber, M. Maio, L. Rivoltini and S. Fais, *PLOS ONE*, 2009, **4**, e5219.
38. A. Riches, E. Campbell, E. Borger and S. Powis, *Eur. J. Cancer*, 2014, **50**, 1025-1034.
39. J. Van Deun, P. Mestdagh, R. Sormunen, V. Cocquyt, K. Vermaelen, J. Vandesompele, M. Bracke, O. De Wever and A. Hendrix, *J. Extracell. Vesicles*, 2014, **3**, 24858.
40. D. S. Abou, D. L. J. Thorek, N. N. Ramos, M. W. H. Pinkse, H. T. Wolterbeek, S. D. Carlin, B. J. Beattie and J. S. Lewis, *Pharm. Res.*, 2013, **30**, 878-888.
41. M. Reifarth, D. Pretzel, S. Schubert, C. Weber, R. Heintzmann, S. Hoeppener and U. S. Schubert, *Chem. Commun.*, 2016, **52**, 4361-4364.
42. P. Charoenphun, L. K. Meszaros, K. Chuamsaamarkkee, E. Sharif-Paghaleh, J. R. Ballinger, T. J. Ferris, M. J. Went, G. E. D. Mullen and P. J. Blower, *Eur. J. Nucl. Med. Mol. Imaging*, 2015, **42**, 278-287.
43. O. P. B. Wiklander, J. Z. Nordin, A. O'Loughlin, Y. Gustafsson, G. Corso, I. Mäger, P. Vader, Y. Lee, H. Sork, Y. Seow, N. Heldring, L. Alvarez-Erviti, C. I. E. Smith, K. Le Blanc, P. Macchiarini, P. Jungebluth, M. J. A. Wood and S. E. L. Andaloussi, *J. Extracell. Vesicles*, 2015, **4**.
44. S. C. Saunderson, A. C. Dunn, P. R. Crocker and A. D. McLellan, *Blood*, 2014, **123**, 208-216.
45. C. Williams, F. Royo, O. Aizpurua-Olaizola, R. Pazos, G.-J. Boons, N.-C. Reichardt and J. M. Falcon-Perez, *J. Extracell. Vesicles*, 2018, **7**, 1442985.
46. M. T. Ma, L. K. Meszaros, B. M. Paterson, D. J. Berry, M. S. Cooper, Y. Ma, R. C. Hider and P. J. Blower, *Dalton Trans.*, 2015, **44**, 4884-4900.
47. T. Tian, H. X. Zhang, C. P. He, S. Fan, Y. L. Zhu, C. Qi, N. P. Huang, Z. D. Xiao, Z. H. Lu, B. A. Tannous and J. Gao, *Biomaterials*, 2018, **150**, 137-149.